Research Article

Journal of Environmental Nanotechnology

Enhanced Adsorptive Removal of Methylene Blue Using Kaolinite–$MnFe_2O_4$ Nanocomposites: Synthesis, Characterization and Adsorption Mechanisms

Manish Patidar[1], Deepak Sharma[1], G. Meena Devi[2], L. R. Sujithra[3*], S. Sathish Kumar[4] and Sumanth Ratna Kandavalli[5]

[1]Department of Electronics and Communication Engineering, Jaypee University of Engineering and Technology, Raghogarh, Guna, MP, India
[2]Department of Mathematics, St. Joseph's College of Engineering, OMR, Chennai, TN, India
[3]Department of Artificial Intelligence and Data Science, Sri Eshwar College of Engineering, Coimbatore, TN, India
[4]Department of Electrical and Electronics Engineering, M. Kumarasamy College of Engineering, Karur, TN, India
[5]Department of Mechanical Engineering, Tandon School of Engineering, New York University, Brooklyn, 6 Metro Tech Center, New York, USA
Received: 22.11.2025 Accepted: 06.02.2026 Published: 30.03.2026
*lrsujithra9@gmail.com

ABSTRACT

Kaolinite (K)-based matrices modified with manganese ferrite nanoparticles ($MnFe_2O_4$) were synthesized via a microwave-assisted route and evaluated as magnetically recoverable adsorbents for methylene blue (MB) removal from aqueous solutions. Structural, morphological, and compositional characteristics were investigated using X-ray diffraction (XRD), X-ray fluorescence (XRF), Fourier transform infrared spectroscopy (FTIR), scanning electron microscopy (SEM), and Brunauer–Emmett–Teller (BET) surface area analysis. XRD confirmed the presence of inverse spinel $MnFe_2O_4$, while XRF revealed a significant increase in iron oxide content, indicating successful incorporation of manganese ferrite into the kaolinite matrix. FTIR and SEM analyses supported surface modification through changes in functional groups and morphology. Batch adsorption studies demonstrated that MB removal efficiency was influenced by solution pH, adsorbent dosage, initial dye concentration, contact time, and temperature. Optimal adsorption performance was achieved at pH 5, an initial MB concentration of 40 mg/L, and an adsorbent dosage of 0.6 g/L, attaining approximately 91% removal efficiency. Adsorption equilibrium was best described by the Langmuir isotherm, indicating monolayer adsorption on a homogeneous surface. Kinetic data followed the pseudo-second-order model, suggesting that the adsorption rate was governed by surface interaction mechanisms rather than diffusion control. Thermodynamic analysis revealed that the adsorption process was spontaneous and weakly exothermic, with enhanced adsorption at elevated temperatures attributed to improved mass transfer rather than thermodynamic favorability. The $MnFe_2O_4$-modified kaolinite exhibited superior adsorption capacity and magnetic separability compared with natural kaolinite, along with good regeneration performance over multiple cycles. These findings demonstrate that $MnFe_2O_4$-embedded kaolinite matrices are promising, low-cost, and reusable adsorbents for dye-contaminated wastewater treatment.

Keywords: Adsorption; Langmuir isotherm; Kaolinite; Crystal structure; Thermodynamic analysis.

1. INTRODUCTION

The discharge of synthetic dyes, such as methylene blue (MB), into aquatic environments poses serious environmental and health risks due to their toxicity, high visibility, and resistance to natural degradation. MB is extensively used in textile, paper, leather, and pharmaceutical industries, and its presence in wastewater can inhibit light penetration, disrupt photosynthetic activity, and pose risks to aquatic organisms. Consequently, the development of efficient and sustainable methods for MB removal from wastewater remains a critical research priority. The chemical structure of MB is illustrated in Fig. 1.

Among the available treatment techniques, adsorption is widely recognized as an effective and economical approach because of its operational simplicity, adaptability, and high removal efficiency. In adsorption-based dye removal, mechanisms such as electrostatic interaction, surface complexation, and hydrogen bonding play a dominant role in governing adsorbate–adsorbent interactions (Rao *et al.* 2025). In this context, biosorbents have gained increasing attention. For example, *Tamarindus indica* seed gum–grafted materials demonstrated effective pollutant removal, following the Langmuir and Freundlich isotherms with good reusability (Sharmiladevi *et al.* 2024). Natural clay minerals, particularly kaolinite, montmorillonite, and vermiculite, have been extensively investigated as low-cost and environmentally benign adsorbents because of their abundance, layered structure, and surface hydroxyl groups (Barbosa *et al.* 2023).

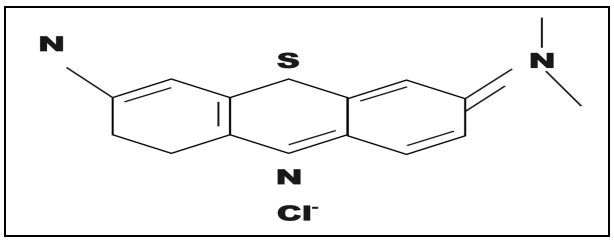


Fig. 1: Chemical structure of methylene blue

Natural clay minerals, particularly kaolinite, have attracted significant attention as low-cost adsorbents due to their abundance, chemical stability, and surface hydroxyl functionalities. Several studies have reported the ability of raw kaolinite and kaolinite-rich clays to adsorb MB through electrostatic attraction between cationic dye molecules and negatively charged clay surfaces (Subhi *et al.* 2022; Babakr *et al.* 2025; Loukili *et al.* 2021). Nevertheless, pristine kaolinite generally exhibits moderate adsorption capacity because of its relatively low specific surface area and limited number of accessible adsorption sites, which restrict its practical application in high-strength dye wastewater. Green-synthesized metal oxide nanoparticles, such as CuO, Fe_2O_3, and $CuFeO_2$, have also shown favorable physicochemical properties for environmental remediation (Mussttaf *et al.* 2024).

To overcome these limitations, various modification strategies have been explored to enhance the adsorption performance of kaolinite-based materials. Acid activation, thermal treatment, and surface functionalization have been shown to improve porosity and surface reactivity, leading to higher MB uptake (Sandollah *et al.* 2020). Similarly, clay–biopolymer composites, such as kaolinite–moringa seedcake and chitosan–kaolinite systems, have demonstrated improved dye removal efficiencies by introducing additional functional groups and enhancing surface interactions (Rawat and Ahammed, 2024; Biswas *et al.* 2020). While these approaches enhance adsorption capacity, they often require high adsorbent dosages or exhibit reduced stability after repeated use. Several investigations have reported adsorption kinetics following pseudo-second-order models and equilibrium behavior consistent with Langmuir or Freundlich isotherms, suggesting surface-interaction-controlled adsorption processes (Jiang *et al.* 2024; Ata *et al.* 2022). Nevertheless, many of these systems require high adsorbent dosages or involve complex synthesis procedures, limiting their practical applicability.

Other advanced treatment strategies, including combined adsorption–Fenton oxidation, photocatalysis, and hybrid adsorption–nanofiltration systems, have also been investigated for dye removal (Milojević-Rakić *et al.* 2024; Sharma *et al.* 2022; Harinivalli *et al.* 2025). In parallel, metal oxide incorporation into clay matrices has been widely investigated to further improve adsorption efficiency. Kaolinite-based composites containing oxides such as TiO_2, Fe_2O_3, and ZnO have been reported to enhance dye removal through increased surface area and improved surface reactivity (Barbosa *et al.* 2023; Suliman *et al.* 2024; Choudhary *et al.* 2023). Although some of these materials also exhibit photocatalytic or antibacterial activity, their relevance to dye adsorption is primarily associated with improved surface properties rather than catalytic degradation. Moreover, photocatalytic systems often require external light sources and may suffer from catalyst recovery challenges, limiting their applicability in adsorption-focused wastewater treatment.

Magnetic modification of clay-based adsorbents has emerged as an effective strategy to address separation and reusability issues. The incorporation of magnetic nanoparticles such as Fe_3O_4 or ferrite phases into kaolinite matrices enables facile magnetic recovery while simultaneously enhancing adsorption performance (Shikuku and Mishra, 2021; Liu *et al.* 2020). Several magnetic clay composites have demonstrated improved MB removal efficiency along with better recyclability compared to non-magnetic counterparts. However, many reported magnetic adsorbents are synthesized via multistep or energy-intensive routes, and their adsorption mechanisms and thermodynamic behavior are often inconsistently interpreted.

Manganese ferrite ($MnFe_2O_4$), an inverse spinel ferrite, has attracted growing interest as a modifier due to its magnetic properties, chemical stability, and potential to enhance adsorption through surface heterogeneity. While $MnFe_2O_4$-based composites have been investigated for the removal of various contaminants, including dyes and heavy metals (Hosseini-Bandegharaei *et al.* 2025), studies specifically focusing on MB adsorption using $MnFe_2O_4$-modified kaolinite remain limited. In particular, there is a lack of systematic investigations employing energy-efficient synthesis methods that combine enhanced adsorption capacity, magnetic separability, and reusability. While kaolinite-based magnetic composites show promising adsorption performance, challenges remain regarding large-scale applicability and treatment of diverse pollutants beyond model dyes. Most reported studies are limited to batch-scale experiments under controlled laboratory conditions, and broader validation under realistic wastewater matrices is still required. Therefore, the present study focuses on establishing fundamental adsorption behavior and regeneration performance as a basis for future scalability assessment.

Microwave-assisted synthesis has recently emerged as a promising alternative to conventional heating methods, offering rapid reaction rates, improved particle dispersion, reduced energy consumption, and enhanced material homogeneity. Despite these advantages, the application of microwave irradiation for

the synthesis of kaolinite–$MnFe_2O_4$ composites tailored for MB adsorption has not been adequately explored. In this study, kaolinite-based matrices modified with manganese ferrite nanoparticles (hereafter referred to as $MnFe_2O_4$–K composites) were synthesized using a microwave-assisted approach and evaluated as adsorbents for methylene blue removal from aqueous solutions. The effects of pH, adsorbent dosage, initial dye concentration, contact time, and temperature were systematically investigated. Adsorption equilibrium, kinetic, and thermodynamic analyses were performed, and the reusability of the magnetic adsorbent was assessed. This work aims to address the gap by developing a magnetically recoverable, microwave-synthesized kaolinite–$MnFe_2O_4$ adsorbent with improved performance and practical applicability for dye-contaminated wastewater treatment.

Table 1. Structure and physicochemical properties of methylene blue

Parameter	Details
Molecular Formula	$C_{16}H_{18}ClN_3S$
IUPAC Name	3,7-bis(dimethylamino)phenothiazin-5-ium chloride
Synonyms	Methylene blue; CAS No. 61-73-4; Basic Blue 9; methylthioninium chloride
CAS Number	61-73-4
Parent Compound	CID 4139 (methylene blue cation)
Molecular Weight	3.19.85 g/mol
Appearance	Blue powder or crystalline solid
Solubility	Soluble in water
Melting Point	100–110 °C
Boiling Point	Decomposes at > 100° C
pH of Solution	Typically, 3–6 for a 1% solution
UV/Vis Absorption Max	664 nm (in water)
Molar Absorptivity	High (significant absorbance at 664 nm)

2. MATERIALS AND METHODS

2.1 Chemicals and Reagents

Methylene blue (MB, $C_{16}H_{18}ClN_3S$, ≥99% purity) was used as the model cationic dye and was procured from a commercial supplier. Iron (III) chloride hexahydrate ($FeCl_3·6H_2O$, ≥97% purity) and iron (II) sulfate heptahydrate ($FeSO_4·7H_2O$, ≥97% purity) were employed as precursor salts for manganese ferrite synthesis. Sodium hydroxide (NaOH, ≥98%) and hydrochloric acid (HCl, 37%) were procured from Merck, India. Ethanol (analytical grade, ≥99.5%) and deionized water were used as solvents throughout the experiments. All chemicals were used as received without further purification. All stock solutions were formulated by dissolving precise quantities of these chemicals in deionized water.

The kaolinite-based matrices utilized in this work were manufactured through a systematic approach to ensure uniformity in particle size and quality. Raw kaolinite was initially dried at 105 °C for 24 h to remove physically adsorbed moisture. The dried material was then mechanically milled using a planetary ball mill (Retsch PM 100) operated at 300 rpm for 2 h. The milled powder was subsequently sieved using a standard sieve shaker to obtain particles with sizes ≤ 40 µm, which were used for all further experiments. The structural and physicochemical characteristics of MB, which directly affect its adsorption behavior, are presented in Table 1. The chemical formula ($C_{16}H_{18}C_lN_3S$), molecular weight (319.85 g/mol), and solubility are essential for understanding its interaction with adsorbents such as $MnFe_2O_4$.

2.2 Synthesis of Kaolinite-based Matrices Modified with Manganese Ferrite Nanoparticles

For the synthesis, 5 g of $FeCl_3·6H_2O$and 2.3 g of $FeSO_4·7H_2O$ were precisely measured to attain the requisite stoichiometry (2:1). The selected quantities of $FeCl_3·6H_2O$ and $FeSO_4·7H_2O$ correspond to a Fe^{3+}:Fe^{2+} molar ratio of approximately 2:1, which is required to achieve the stoichiometric composition of inverse spinel $MnFe_2O_4$ and is commonly adopted for ferrite formation via co-precipitation. Nitrogen purging was employed throughout the synthesis to prevent oxidation of Fe^{2+} ions to Fe^{3+} during co-precipitation, thereby ensuring proper stoichiometric control and facilitating the formation of phase-pure $MnFe_2O_4$ with consistent magnetic and structural properties. A 250 mL solution of N_2-saturated distilled water was created by infusing nitrogen gas into distilled water for around 30 min, thereafter closing the container to preserve saturation. The reagents were then transferred into an appropriate reaction vessel compatible with the ETHOS EASY system and stirred to achieve homogeneity. The reaction vessel was placed in the ETHOS EASY system, secured, and exposed to microwave irradiation under the following conditions: power, 300 W; duration, 10 min; temperature, 60 °C; ramp rate, 5 °C/min; and hold duration, 10 min. Microwave irradiation was applied both before and after kaolinite addition in a two-step process. Initially, precursor iron salt solutions were subjected to microwave irradiation to promote nucleation of manganese ferrite

($MnFe_2O_4$) nanoparticles. Following irradiation, the pH of the solution was elevated to above 8.5 with a sodium hydroxide solution. Pre-treated kaolinite was then added to the reaction mixture at a fixed mass ratio of kaolinite: $MnFe_2O_4$ = 2:1, and the suspension was subjected to additional microwave irradiation under identical conditions to promote the uniform deposition of $MnFe_2O_4$ onto the kaolinite surface. The resultant black solid residue was isolated using centrifugation and washed with deoxygenated distilled water and anhydrous ethanol to eliminate contaminants. The pure manganese ferrite crystals were subjected to vacuum drying at 60 °C overnight to eliminate any residual solvent.

2.3 Determination of the Adsorbent's Point of Zero Charge

The pH at which the surface charge of raw kaolinite-based matrices and manganese ferrite nanoparticles within kaolinite-based matrices ($MnFe_2O_4$–K) attains neutrality was determined using the following methodology: The point of zero charge (pH ZPC) of raw kaolinite and the $MnFe_2O_4$–kaolinite composite was determined using the pH drift method. A series of 0.1 M NaCl solutions (50 mL) was adjusted to initial pH values ranging from 3 to 12 using 0.1 M HCl or NaOH. Subsequently, 0.3 g of adsorbent was added to each solution and agitated for 24 h at room temperature to allow surface charge equilibration. After equilibration, the final pH (pH_f) of each suspension was measured. The difference between initial and final pH values ($\Delta pH = pH_f - pH_i$) was plotted against the initial pH (pH_i). The pH at which ΔpH equals zero was identified as the point of zero charge (pH ZPC) of the material. This value represents the pH at which the net surface charge of the adsorbent is neutral.

2.4 Characterization Techniques and Instruments

Advanced analytical approaches were utilized to obtain the composition of kaolinite-based matrices and kaolinite-based matrices modified with manganese ferrite nanoparticles ($MnFe_2O_4$–K). The crystalline structure was analyzed using XRD with Cu Kα radiation (λ = 1.5406 Å). Diffraction patterns were recorded over a 2θ scan range of 10–80° with a step size of 0.02° and a scanning rate of 2° min^{-1}, operating at 40 kV and 30 mA. Surface morphology and microstructural features were examined using SEM, conducted at an accelerating voltage of 10–15 kV, with images acquired at various magnifications ranging from 5,000× to 50,000× to evaluate particle distribution and surface texture. Elemental composition was analyzed using the EDS attached to the SEM system. Specific surface area, pore volume, and pore size distribution were determined by BET nitrogen adsorption–desorption analysis. Before measurements, all samples were degassed at 150 °C for 6 h under vacuum to remove physically adsorbed moisture and gases. Nitrogen adsorption measurements were carried out at 77 K, and BET surface area values were calculated from adsorption data in the relative pressure (P/P_0) range of 0.05–0.30.

2.5 Efficacy of Adsorption

This study involved adsorption tests to assess the efficacy of $MnFe_2O_4$ as an adsorbent. The adsorption tests were performed in a basic batch method utilizing a 500 mL borosilicate glass round-bottom flask. The experiments were structured by manipulating critical parameters, including pH levels (1, 2, 3, 4, 5, 7, and 9), initial adsorbate concentrations (20, 40, 60, and 80 mg/L), adsorbent doses (0.1, 0.2, 0.4, and 0.6 g/L), temperatures (20, 30, 40, 50, and 60 °C), and contact durations (10, 20, 30, 40, 50, 60, 70, 80, 90, and 100 min). The flask was affixed to a bath stirrer to facilitate adequate mixing of the solution at designated reaction intervals. The mixes were further filtered through a 0.45 µm filter paper to exclude any particles that would interfere with the analysis. Each experiment was conducted in triplicate, and the findings were averaged. Subsequently, 10 mL of the solution was extracted and then analyzed in a spectrophotometer at a wavelength of 664 nm. The standard deviation (SD) was calculated to evaluate the repeatability of the results. The removal effectiveness of adsorption (RE%) was computed according to the specified method. This parameter optimization offers critical insights into the optimal circumstances for employing $MnFe_2O_4$ in the adsorption process, emphasizing its efficacy across diverse experimental situations.

2.6 Regeneration of Kaolinite-based Matrices and Manganese Ferrite Nanoparticle-modified Kaolinite-based Matrices

The regeneration procedure for $MnFe_2O_4$–K was developed to facilitate the reutilization of exhausted materials across several adsorption cycles. The wasted $MnFe_2O_4$ particles were initially collected using separation methods, such as centrifugation or magnetic decantation. The gathered particles were further rinsed meticulously with distilled water to eliminate weakly attached contaminants and any remaining adsorbate (e.g., methylene blue). Subsequent to the washing phase, chemical regeneration was performed by treating the exhausted $MnFe_2O_4$-modified kaolinite with a 0.1 M KCl solution to promote ionic strength–assisted desorption of methylene blue, followed by thorough rinsing with deionized water.

Following chemical treatment, the particles were thoroughly rinsed several times with distilled water to remove any residual regenerating agents. To regenerate kaolinite-based matrices, the purified manganese ferrite nanoparticles were re-modified by activating their surface through a modest acid treatment

(e.g., 0.01 M HCl) to restore surface reactivity. Thereafter, the activated nanoparticles were combined with fresh kaolinite-based matrices in an aqueous medium while maintaining continual agitation to facilitate bonding. The regenerated $MnFe_2O_4$ was subsequently rinsed with deionized water and then dried at 60 °C until consistent weights were attained. The reusability of the $MnFe_2O_4$-modified kaolinite was assessed over five adsorption–desorption cycles. After each adsorption run, the spent adsorbent was magnetically separated and washed with deionized water. Desorption was performed using 0.1 M KCl at a solid–liquid ratio of 1 g L^{-1} for 60 min at room temperature, followed by rinsing and drying at 60 °C before reuse.

Table 2. XRF elemental composition (wt.%), BET surface area, pore characteristics, and particle size distribution of kaolinite-based matrices and $MnFe_2O_4$-modified kaolinite-based matrices

Content		Kaolinite-based Matrices (wt.%)	$MnFe_2O_4$–K
Al_2O_3 (wt.%)		22.64 ± 0.05	15.65 ± 0.02
SiO_2 (wt.%)		52.22 ± 0.05	56.34 ± 0.03
Fe_2O_3 (wt.%)		2.17 ± 0.21	18.28 ± 0.01
CaO (wt.%)		2.05 ± 0.8	1.75 ± 0.01
Na_2O (wt.%)		1.42 ± 0.02	0.52 ± 0.01
K_2O (wt.%)		1.39 ± 0.56	1.32 ± 0.01
MgO (wt.%)		2.45 ± 0.11	1.54 ± 0.02
SO_3 (wt.%)		0.18 ± 0.01	0.07 ± 0.01
Surface area (m^2 g^{-1}) by BET		87.87	131.25
Pore radius (Å)		15.03	14.95
Pore volume ($\times 10^{-3}$ L g^{-1})		0.019	0.041
Particle size distribution (%)	Clay (< 2 µm)	79.55	82.19
	Silt (2–63 µm)	14.95	14.92
	Sand (> 63 µm)	5.5	2.89

Quality control assessments were performed to evaluate the regeneration efficiency, which involved evaluating the adsorption capacity of regenerated $MnFe_2O_4$ and comparing it to the original material.

3. RESULTS AND DISCUSSION

3.1 Characteristics of Kaolinite-based Matrices and Manganese Ferrite Nanoparticle-modified Kaolinite-based Matrices

Table 2 demonstrates substantial alterations in the elemental composition of kaolinite-based matrices following treatment with manganese ferrite nanoparticles ($MnFe_2O_4$). The iron oxide content (Fe_2O_3) significantly escalates from 2.17 wt.% to 18.28 wt.%, hence augmenting the magnetic characteristics of the material. The significant rise in iron oxide is expected to enhance the adsorption ability of $MnFe_2O_4$ for pollutants like methylene blue. Simultaneously, the aluminum oxide (Al_2O_3) concentration diminishes from 22.64 wt.% to 15.65 wt.%, potentially influencing the structural and adsorption properties of the material. The silicon oxide (SiO_2) content increases from 52.22 wt.% to 56.34 wt.%, suggesting maintained or enhanced surface area, advantageous for adsorption. The reductions in calcium oxide (CaO), sodium oxide (Na_2O), magnesium oxide (MgO), and sulfate (SO_3) are comparatively negligible and less significant than the augmented iron content. The increased presence of iron oxide in $MnFe_2O_4$ is anticipated to markedly enhance its efficacy as an adsorbent.

The XRD pattern of raw kaolinite exhibited characteristic diffraction peaks at 2θ values of approximately 12.3°, 20.1°, and 24.8°, corresponding to the (001), (020), and (002) planes of triclinic kaolinite, which are consistent with JCPDS Card No. 14-0164, as shown in Fig. 2(a). For the $MnFe_2O_4$-modified kaolinite sample, additional diffraction peaks observed at 2θ ≈ 30.2°, 35.5°, 43.2°, 57.1°, and 62.7° were indexed to the (220), (311), (400), (511), and (440) crystal planes of cubic spinel $MnFe_2O_4$ in Fig. 2(b), matching well with JCPDS Card No. 10-0319. The absence of impurity peaks confirms the successful formation of phase-pure $MnFe_2O_4$ within the kaolinite matrix. Similarly, in the previous studies, XRD analysis confirmed the crystalline structure and phase purity of the synthesized nano-ceramic clays. The sharp diffraction peaks indicated high crystallinity for kaolinite, validating their nanoscale formation (Yadav *et al.* 2025).

Table 2 shows the surface area, pore attributes, and particle size distribution of natural kaolinite matrices with those modified by $MnFe_2O_4$ nanoparticles. The BET surface area of $MnFe_2O_4$ is markedly greater at 131.25 m^2/g compared to 87.87 m^2/g for natural kaolinite-based matrices, signifying an enhanced surface area for adsorption. The enhanced adsorption performance of $MnFe_2O_4$-modified kaolinite arises not only from increased surface area but also from altered surface charge characteristics and additional active sites that strengthen electrostatic interactions with methylene blue. The pore radius slightly decreased, while the pore

volume increased in $MnFe_2O_4$-modified kaolinite-based matrices (14.95 Å and 0.041 L g^{-1}, respectively) compared to natural kaolinite-based matrices (15.03 Å and 0.019 L/g), indicating that manganese ferrite alteration enhances the adsorbent capacity. Although a slight decrease in pore radius (15.03 Å to 14.95 Å) was observed after $MnFe_2O_4$ modification, the significant increase in surface area and pore volume suggests enhanced adsorption potential, rather than pore size reduction alone. Regarding particle size distribution, $MnFe_2O_4$ exhibits a minor increase in the clay fraction (2 µm), which diminishes from 5.5% to 2.89%. The transition to smaller particles in $MnFe_2O_4$ likely enhances its adsorption capabilities by increasing surface area and pore volume for contaminant interaction. In previous studies, BET analysis showed a high surface area of 442.57 m^2/g with a pore diameter of 2.36 nm. These results indicate a mesoporous structure, enhancing adsorption and photocatalytic efficiency (Mohammad *et al.* 2025).

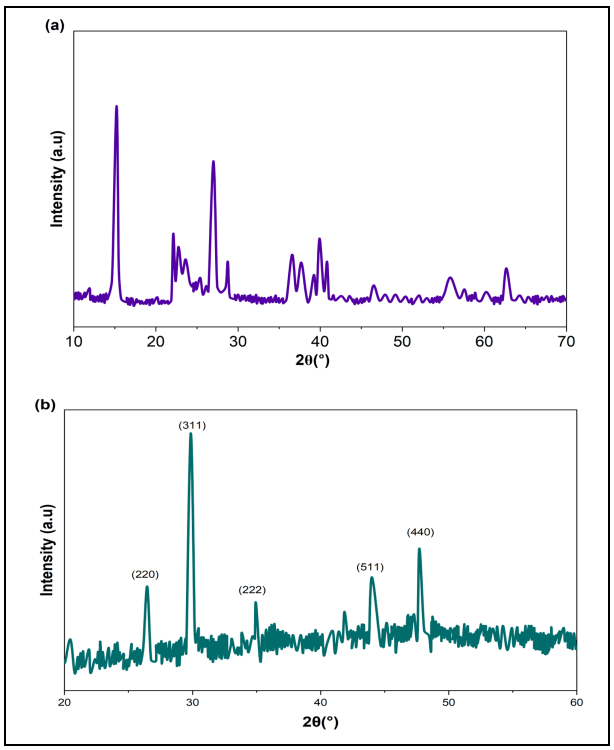


Fig. 2: XRD patterns of (a) kaolinite-based matrices and (b) $MnFe_2O_4$-modified kaolinite-based matrices

The broad absorption band observed in the region 3200–3700 cm^{-1} corresponds to O–H stretching vibrations associated with surface hydroxyl groups and adsorbed water molecules. The band near 1630–1650 cm^{-1} is attributed to H–O–H bending vibrations of physically adsorbed water. These assignments are consistent with kaolinite-based materials (Fig. 3a). Absorption bands seen in wave numbers 886.03 and 1112.24 cm^{-1} exhibit the vibration Si–O– characteristic uptake of kaolinite materials. The peak of absorption region 3656.16 cm^{-1} shows the presence of –OH vibrations with environmental changes of -OH bonded to Al octahedral atoms at inter-layer silicate or at the surface. The observed wavenumbers were consistent with the kaolinite spectrum: 1596.33 cm^{-1} (–OH bending vibration), 3819.67 cm^{-1} (octahedral –OH stretching vibration), and 886.03 and 1035 cm^{-1} (Si–O vibrations).

The spectrum in the manganese ferrite-modified nanoparticles (Fig. 3b) clearly indicated the distinctive bands of the material at regions connected with precursor materials. The bands in the regions 475.62–575.15 cm^{-1} and 755.48–955.19 cm^{-1} correspond to Fe–O and Mn–O vibrations, respectively. The low-intensity bands in the regions 1178.82–1662.91 cm^{-1}, 2874.76 cm^{-1}, 2941.33 cm^{-1}, and 3340.11–3739.53 cm^{-1} are attributed to vibrations at O–H bonds. The spectral shifts validated the chemical modification of cellulose into the functionalized adsorbent (Saad and Mahmoud, 2025). In this research, the characterization and synthesis of zinc oxide composites with other substances that have Fe–O bonds produced a spectrum of high resemblance.

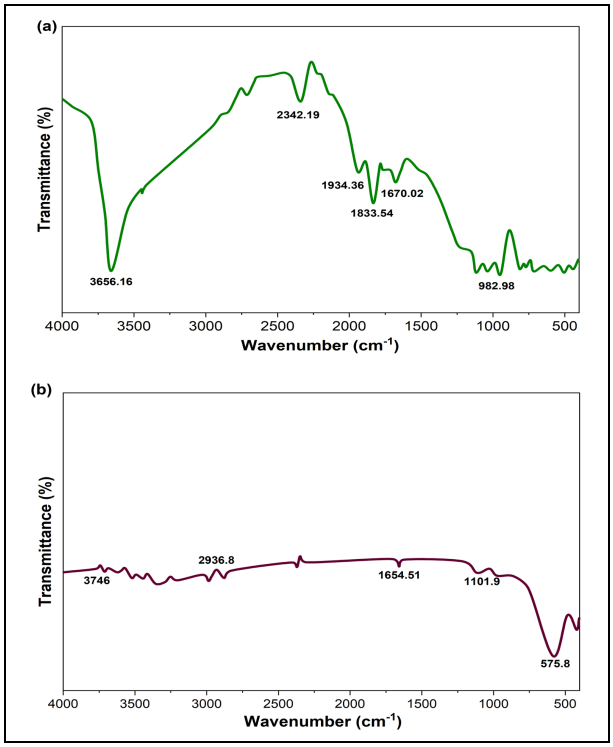


Fig. 3: FTIR spectra of (a) kaolinite-based matrices and (b) manganese ferrite modification nanoparticles with kaolinite

The FTIR spectra demonstrate the changes in kaolinite-based matrices induced by manganese ferrite nanoparticles. The variations and new peaks in Fig. 3b compared to Fig. 3a indicate structural and compositional modifications due to manganese ferrite incorporation, confirming the effectiveness of the modification procedure.

The SEM images show a comparative study of kaolinite-based matrices (Fig. 4a) and those treated with manganese ferrite (Fig. 4b). The raw kaolinite-based matrices have a highly compact, dense structure with smaller, more aggregated particles, and small light crystallites were seen on the sample's surface, perhaps comprising free material. This signifies a comparatively small surface area, with particles densely arranged, restricting the accessibility of active sites required for adsorption. Conversely, the SEM image designated as Fig. 4b of the manganese ferrite-modified kaolinite matrices has a more porous and stratified structure characterized by larger and more prominent particles. The incorporation of manganese ferrite appears to have dramatically modified the surface morphology, resulting in enhanced surface roughness and potentially an increased surface area. The modifications to manganese ferrite indicate an enhancement in the material's adsorption capacity by increasing the number of active sites and improving interactions with adsorbates, which may be essential for applications like pollution removal in water treatment.

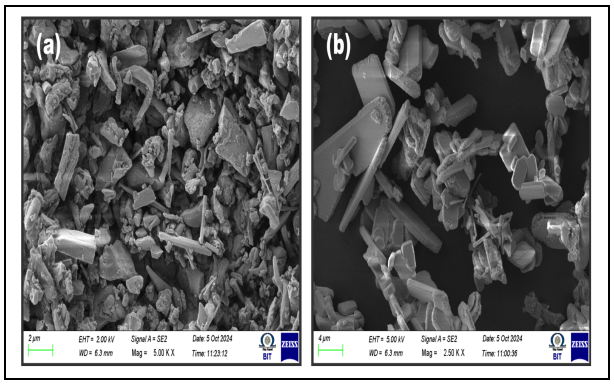


Fig. 4: SEM images of (a) kaolinite-based matrices and (b) modified kaolinite-based matrices

The EDX study of untreated kaolinite-based matrices indicated a composition mostly of oxygen (50%), silicon (25.6%), and aluminum (7.64%), hence affirming its aluminosilicate characteristics. Furthermore, minor quantities of exchangeable cations were identified, including sodium (0.74%), magnesium (2.82%), potassium (0.32%), calcium (0.88%), and iron (1.05%). The surface of untreated kaolinite-based matrices displayed a porous texture, enhancing adsorption at positively charged ion active sites. The clay particles formed heterogeneous aggregates of varying sizes and shapes, resembling stacked layers or sheets. Small crystallites on the surface likely comprised free silica. The EDX analysis confirms the presence of Fe and Mn elements associated with the spinel ferrite $MnFe_2O_4$ phase, along with Si and Al originating from the kaolinite matrix. Minor concentrations of exchangeable cations, including sodium (0.9%), magnesium (1.2%), potassium (0.22%), calcium (0.32%), and iron (1.1%) were detected.

The determination of pH ZPC is a critical metric for comprehending the surface reactivity and electrochemical properties of the materials being studied. Fig. 5 presents a bar graph depicting the disparity between initial and final pH values for both raw kaolinite-based matrices and manganese ferrite nanoparticle-treated kaolinite-based matrices at different initial pH levels. The findings demonstrate that at reduced pH levels (2–4), both materials elevate the pH, with raw kaolinite-based matrices exhibiting a more pronounced increase than those treated with manganese ferrite. As the pH nears neutrality (about 7–8), the pH difference stabilizes around zero, indicating that this range may signify the zero point of charge (pH ZPC) for both substances. At elevated pH values (8–11), the final pH decreases below the initial pH, especially for unprocessed kaolinite-based matrices, signifying a more pronounced acidification action. These observations indicate that the integration of manganese ferrite nanoparticles modifies the surface features of kaolinite matrices, altering their pH behavior and perhaps affecting their adsorption characteristics.

Fig. 5 indicates that the pH ZPC for both materials is between 6.98 and 8.14. Moreover, analysis of the effect of solution concentration on pH ZPC revealed that the value remains consistent across all concentrations, confirming its reliability as a characteristic property of the materials.

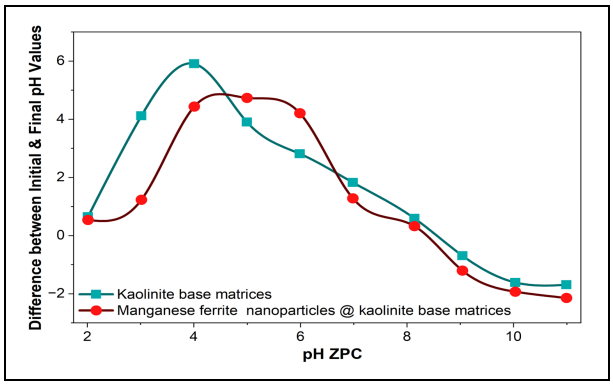


Fig. 5: pH ZPC for kaolinite-based matrices and manganese ferrite nanoparticles at kaolinite-based matrices

3.2 Adsorption Processes

3.2.1 Effect of Material Dosage

This study examined the effect of altering the dosage of manganese ferrite nanoparticles embedded in kaolinite matrices ($MnFe_2O_4$–K) from 0.1 to 0.6 g/L on the adsorption of a 40 mg/L methylene blue (MB) solution. The trials were performed under defined conditions: agitation at 300 rpm, a pH of 7, and a temperature of 30 °C. Fig. 6 illustrates a significant trend where adsorption efficiency escalates with increasing dosage, peaking at 0.6 g/L. This tendency results from the

augmented number of active sites due to elevated $MnFe_2O_4$ doses, which improves the contact surface area between the adsorbent and the contaminants. At elevated doses, the augmented surface area and accessibility of sites lead to a corresponding enhancement in adsorption efficiency. In addition to surface area enhancement, the modification introduces Fe–O surface sites that contribute to stronger adsorbate–adsorbent interactions. This discovery indicates that an increased quantity of adsorbent correlates with a higher adsorption rate, owing to the augmented availability of surface sites for interaction with the adsorbate. The ideal dosage of $MnFe_2O_4$ for effective MB adsorption is established as 0.6 g/L. Thermally activated kaolinite optimized by RSM achieved 97.8 mg/g methylene blue removal. Adsorption kinetics followed a pseudo-second-order model, while equilibrium data were well described by the Freundlich isotherm. The regenerated adsorbent maintained high efficiency and structural stability (Karuppaiyan *et al.* 2023).

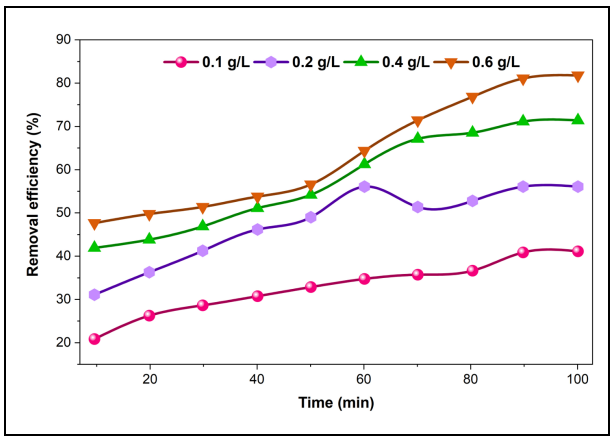


Fig. 6: Impact of dosage on MB adsorption

3.2.2 Effect of pH

Fig. 7 depicts the effect of pH on the removal efficiency of MB across several pH levels (pH 1, pH 2, pH 3, pH 4, pH 5, pH 7, and pH 9). The data indicate that removal effectiveness markedly enhances in neutral to slightly alkaline conditions, especially at pH levels 5 and 7. This trend indicates that the adsorption of MB is more advantageous under these conditions, perhaps owing to the deprotonation of functional groups at the adsorbent surface and cationic MB molecules. The findings are consistent with the pH ZPC analysis shown in Fig. 7, which indicates that the adsorbent's pH ZPC is approximately 5, above which the surface becomes negatively charged. At this pH, the adsorbent's surface possesses a net negative charge, reducing electrostatic repulsion and enhancing MB adsorption. This further substantiates the idea that hydrogen bonding and electrostatic interactions between methylene blue and surface groups such as Si–OH and Al–OH on kaolinite matrices are pivotal in the adsorption process.

At reduced pH levels, the solution acquired a positive charge, leading to competition among hydrogen ions and positively charged MB cations for active adsorption sites. At elevated pH levels (exceeding pH 5), the deprotonation of the adsorbent surface produces a negatively charged surface that interacts robustly with neutral or positively charged MB molecules, hence sustaining high removal efficiency. Similarly, magnetic halloysite–chitosan nanocomposites (MHNT–CTN) showed 83.9% MB removal at pH 8 with a 2:1 MHNT:CTN ratio. This nanocomposite offered both magnetic separability and high adsorption efficiency (Turkes and Açıkel, 2020). This pH-dependent response underscores the ideal circumstances for MB adsorption and illustrates the essential influence of the charge states of both the adsorbent and adsorbate in the process.

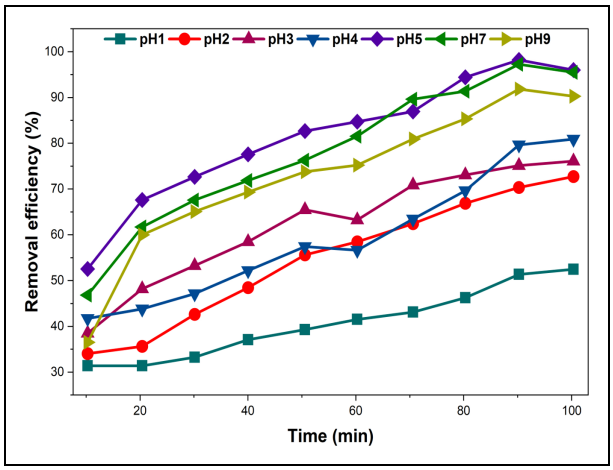


Fig. 7: Effect of solution pH on MB removal efficiency

3.2.3 Influence of Initial Concentration

Fig. 8 illustrates the removal efficiency in relation to various initial concentrations of MB (20 mg/L, 40 mg/L, 60 mg/L, and 80 mg/L). This inquiry was aimed at determining the optimal use of the adsorption system by assessing the adsorption rate relative to substrate concentration. The data suggest that optimal MB elimination effectiveness is attained at an initial concentration of 40 mg/L. Beyond this concentration, the adsorption rate reduces, presumably due to the saturation of accessible adsorption sites and improved competition between MB molecules for these sites, hindering the adsorption process.

Three equilibrium models were employed to describe adsorption behavior: the Langmuir model, which assumes monolayer adsorption; the Freundlich isotherm, characterizing adsorption on heterogeneous surfaces; and the Temkin model, which accounts for the effects of indirect adsorbate–adsorbate interactions. In previous studies, star-fruit-leaf-derived activated carbon (AC) in ZnO nanocomposites effectively removed methylene blue (MB). The combined photocatalytic and

adsorptive properties facilitated superior dye degradation (Jebanisha and Devi, 2025). These models elucidated the adsorption mechanism and the interaction between the adsorbent and methylene blue molecules.

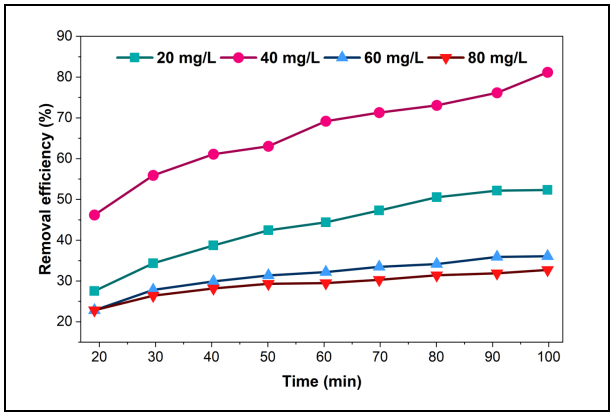


Fig. 8: Effect of initial MB concentration on removal efficiency

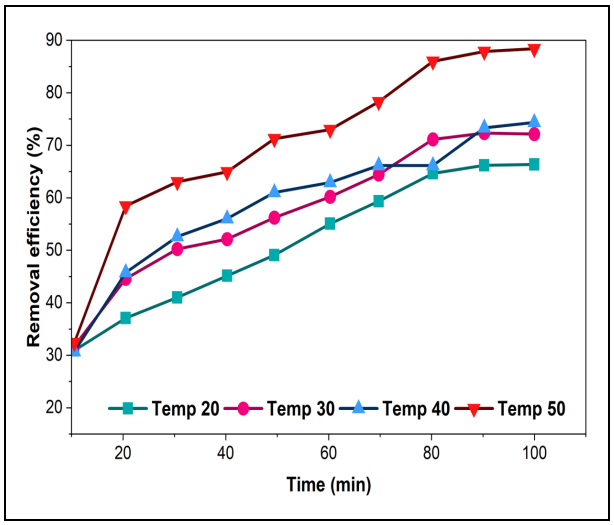


Fig. 9: Impact of temperature

This study assessed the relevance of these isotherms for MB adsorption on $MnFe_2O_4$–K, as illustrated in Table 3 and Fig. 10(a–c). The regression coefficient (R^2) was utilized to identify the optimal isotherm model. The R^2 value demonstrated a robust fit with the Langmuir model (Freundlich: 0.22–0.99, Langmuir: 0.98–0.99, and Temkin: 0.34–0.99). The Langmuir model demonstrated the greatest R^2 values, validating its appropriateness for characterizing MB adsorption on $MnFe_2O_4$.

Table 3 delineates the Langmuir isotherm parameters for the adsorption of MB at different temperatures. Acetic acid-treated *Pithecellobium dulce* (PD) seed pods effectively removed Reactive Red 195-A dye. Adsorption followed the Temkin isotherm and pseudo-second-order kinetics. The process was spontaneous and endothermic, proving PD as a low-cost green adsorbent (Baburao *et al.* 2025). The R^2 values (0.984 to 0.957) indicate a robust correlation with the Langmuir model, substantiating the concept of monolayer adsorption. This pattern is further supported by the Adjusted R^2 values, which range from 0.97 to 0.978, signifying variations in the adsorption equilibrium constant with temperature. The observations demonstrate that although the adsorption capacity increases with elevated temperatures, variations in the equilibrium constant also affect the overall efficacy of MB removal.

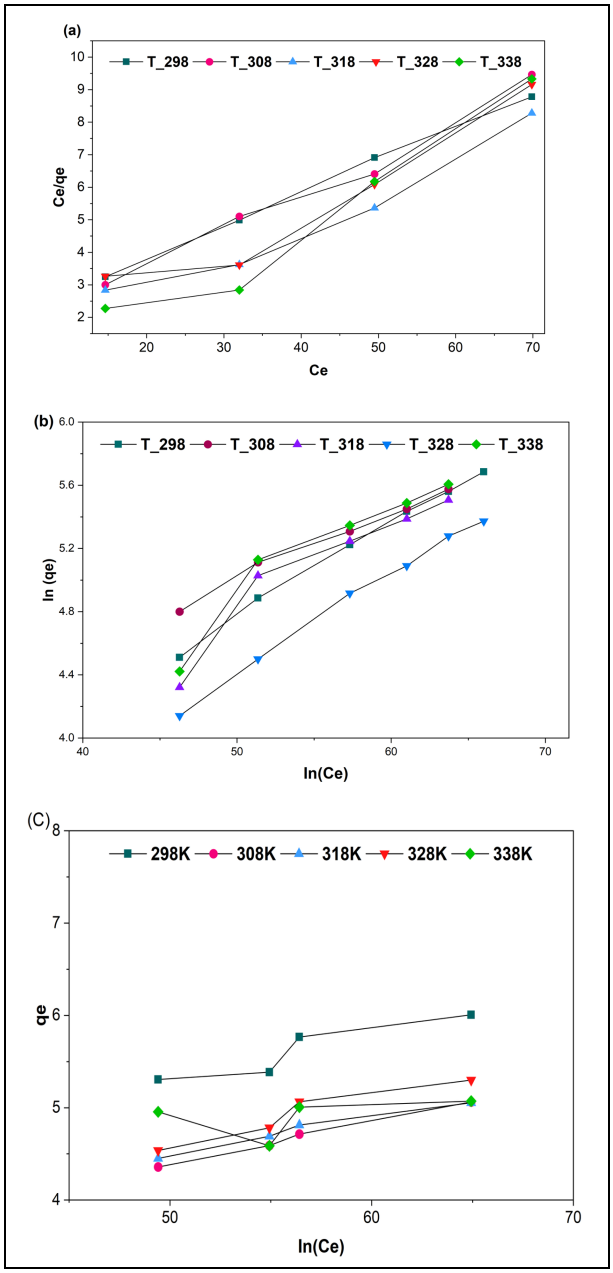


Fig. 10: Adsorption isotherm models of (a) Langmuir, (b) Freundlich and (c) Temkin

Table 3 displays the Freundlich adsorption characteristics for MB at various temperatures. The R^2 values vary from 0.320 to 0.945, indicating a diverse

range of fit among the examined temperatures. Reduced R^2 values signify a diminished accuracy in depicting the adsorption process. The Freundlich exponent (n) has considerable variability, varying from 3.181 to 0.995. At 298 K and 308 K, n values under 1.5 indicate reduced adsorption intensity and a propensity for non-ideal adsorption. Conversely, at elevated temperatures (318 K to 338 K), n rises to a value of 2.98, signifying more advantageous and diverse adsorption conditions.

Table 3. Langmuir, Freundlich, and Temkin isotherm parameters for MB adsorption

Langmuir Equation Variables					
T (K)	298	308	318	328	338
Slope	0.101	0.113	0.099	0.111	0.134
Intercept	1.789	1.285	0.899	0.921	0.424
R^2	0.998	0.984	0.951	0.928	0.945
Adjusted R^2	0.998	0.976	0.976	0.892	0.918
Freundlich Equation Variables					
Temperature, T (K)	298	308	318	328	338
Slope	0.321	0.320	0.317	0.320	0.334
Intercept	1.159	1.115	0.995	3.1242	3.051
R^2	0.997	0.995	0.996	0.992	0.9919
n	3.112	3.124	3.151	3.120	2.980
Kf (L/g)	3.181	3.051	2.893	2.750	2.521
Temkin Equation Variables					
T (K)	-	308	318	328	**338**
Slope	-	0.426	1.16	1.7	0.50
Intercept	-	0.851	0.76	0.5	2.97
R^2	-	0.921	0.98	0.92	0.35
K_T	-	0.73	0.69	0.59	0.55
$\ln K_T$	-	0.31	0.37	0.52	0.60
Values of Thermodynamic Parameters					
1/T	0.0034	0.0033	0.0032	0.0031	0.00305
Gibbs free energy ΔG° kJ mol^{-1}	-4.1	-4.13	-4.19	-4.22	-4.28
R (J/mol K)			8.512		
Entropy ΔS° J mol^{-1} K^{-1}			6.2		
Enthalpy ΔH° kJ mol^{-1}			-1.542		

The Freundlich constant K_f escalates with temperature, indicating enhanced adsorption capacity as temperature increases, with values spanning from 3.18 L/g to 2.52 L/g. The Freundlich model characterizes adsorption as a heterogeneous process; however, the variability in R^2 and n values indicates that it may not reliably represent the adsorption behavior of MB throughout the full temperature range as effectively as the Langmuir model.

Table 3 displays the Temkin adsorption characteristics for MB at different temperatures. The R^2 values vary from 0.35 to 0.98, signifying a generally favorable fit at lower temperatures, but reduced accuracy at elevated temperatures. The Temkin constant K_T escalates with temperature, varying from 0.55 to 0.59, indicating that the heat of adsorption gets increasingly favorable as temperature rises. Correspondingly, the natural logarithm of K_T ($\ln K_T$) exhibits a significant increase, showing a substantial rise in adsorption affinity at elevated temperatures. The low R^2 value of 0.35 at 338 K suggests that the Temkin model's fit deteriorates at elevated temperatures, showing uneven adsorption behavior under these conditions. The Temkin model emphasizes the significance of adsorption heat, which rises with temperature; yet, its reliability is lower than that of the Langmuir model throughout the whole temperature range.

3.2.4 Impact of Temperature on Adsorption

Fig. 11 shows the effect of varying temperatures (20, 30, 40, 50, and 60 °C) on the removal efficiency of MB. The results demonstrate a notable enhancement in adsorption effectiveness at increasing temperatures (40 and 50 °C), suggesting an endothermic process. This behavior is attributed to enhanced mass transfer and diffusion kinetics rather than thermodynamic endothermicity. The negative ΔH° value confirms that the adsorption process is weakly exothermic in nature. Nonetheless, a minor reduction in effectiveness at 60 °C indicates a potential desorption or degradation of adsorption processes at these temperatures. This temperature-dependent activity can be ascribed to multiple factors: elevated thermal energy enabling MB molecules to surmount activation barriers, enlarged pore diameters augmenting adsorption capacity, and enhanced molecular mobility facilitating interaction with adsorption sites. Prior studies have demonstrated that iron tailing waste, rich in hematite, kaolinite, and goethite, can be used for dye removal via adsorption and Fenton processes. Thermal activation at 400 °C enhanced performance, achieving up to 90% MB removal. The material followed pseudo-second-order kinetics, proving its potential as a low-cost adsorbent and catalyst (Grine *et al.* 2025). Furthermore, elevated temperatures alter the adsorption equilibrium, leading to an increased retention of MB molecules on the nanoparticles.

The thermodynamic parameters, comprising Gibbs free energy (ΔG°), enthalpy (ΔH°), and entropy (ΔS°), provide critical insights into the spontaneity and characteristics of the adsorption process, as detailed in Table 3. The parameters were calculated using the equation $\Delta G° = -RT \ln K$, where K denotes the equilibrium constant, over a temperature range of 15 to 40 °C.

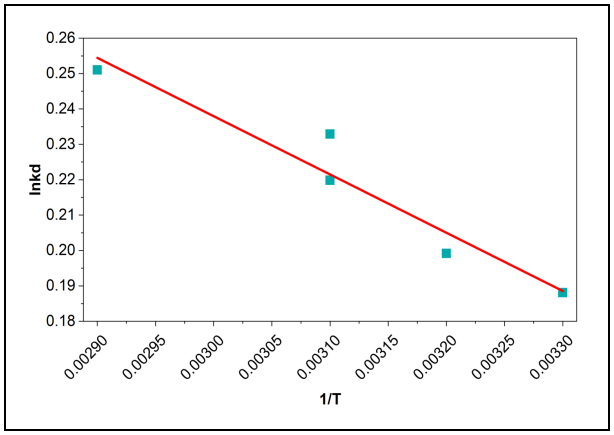


Fig. 11: Correlation between the natural logarithm of K_d and the reciprocal of temperature (1/T)

Table 3 delineates the thermodynamic parameters for MB at various temperatures. The Gibbs free energy change (ΔG°) values, ranging from -4.10 to -4.28 kJ/mol, are uniformly negative, signifying that the adsorption processes were spontaneous. The negative ΔG value indicates that the process is energetically advantageous, facilitating the adsorption of MB onto the adsorbent.

The entropy change (ΔS°) is relatively modest, at 6.2 J mol^{-1} K^{-1}, exhibiting minimal variation across the temperature range, indicating negligible alteration in the adsorption process. The enthalpy change (ΔH°) of −1.358 kJ/mol, obtained from the temperature dependence of ΔG°, signifies that the process was exothermic. The negative enthalpy value shows that adsorption was more advantageous at lower temperatures, aligning with the tendency of increasing ΔG° with elevated temperatures.

The thermodynamic analysis indicates that MB adsorption onto the adsorbent is a spontaneous exothermic process, with negligible effect from entropy variations.

3.3 Recovery or Reusability of Used Materials

Kaolinite-based matrices modified with manganese ferrite nanoparticles ($MnFe_2O_4$–K) were regenerated by a systematic process that includes cleaning, chemical treatment for kaolinite matrix regeneration, re-modification, and quality control to ensure sustainability and efficiency. The regeneration procedure eliminates contaminants from exhausted kaolinite-based matrices and $MnFe_2O_4$ during several adsorption/desorption cycles (six trials) in wastewater treatment. Earlier research demonstrated that a magnetic BCSO/$MnFe_2O_4$ at La-MOF composite removed 99.36% fluoride ions. Adsorption was exothermic and fitted the Langmuir model. High affinity and reusability make it ideal for industrial wastewater treatment (Foroutan *et al.* 2024). The recyclability of kaolinite-based matrices and $MnFe_2O_4$ was assessed under uniform conditions post-recovery. The results indicated a modest drop in removal effectiveness relative to the original material, with decreases of roughly 2–3% for kaolinite-based matrices and $MnFe_2O_4$ when subjected to treatment with 1 M KCl and 5−6 µM Na-2-EDTA.

The adsorption tests were confined to MB, hence limiting the application of the results to other dyes or contaminants. Subsequent investigations should assess the efficacy of $MnFe_2O_4$ against a wider spectrum of pollutants, encompassing heavy metals and organic chemicals. Secondly, scaling up poses a significant challenge; although laboratory results are promising, further research is needed to assess the feasibility, cost-effectiveness, and practicality of industrial-scale implementation. Finally, while preliminary regeneration studies indicated the possibility of reuse, further research is required to assess the long-term stability and efficacy of $MnFe_2O_4$ in practical wastewater treatment applications.

4. CONCLUSION

$MnFe_2O_4$-modified kaolinite was successfully synthesized via microwave-assisted co-precipitation and evaluated for methylene blue adsorption. XRF analysis confirmed an increase in Fe_2O_3 content from 2.17 wt.% in raw kaolinite to 18.28 wt.% in the modified composite. XRD results indicated the preservation of triclinic kaolinite and the formation of cubic spinel $MnFe_2O_4$, confirming phase integrity. FTIR analysis identified Fe–O and Mn–O vibrations characteristic of $MnFe_2O_4$, while SEM revealed morphological changes consistent with nanoparticle deposition. Batch adsorption studies demonstrated optimal removal efficiency (~91%) at pH 5, an initial MB concentration of 40 mg/L, and an adsorbent dosage of 0.6 g/L. Adsorption equilibrium followed the Langmuir model, suggesting monolayer surface coverage, and kinetic behavior was best described by the pseudo-second-order model, indicating surface-interaction-controlled adsorption. The thermodynamic analysis revealed that the process is spontaneous and weakly exothermic ($\Delta H° < 0$). The observed enhancement at moderately elevated temperatures is attributed to improved diffusion kinetics rather than endothermic behavior. The adsorption mechanism is governed primarily by electrostatic interactions and surface complexation between negatively charged adsorbent sites and cationic

methylene blue molecules. Regeneration studies demonstrated stable performance over five adsorption–desorption cycles with minimal efficiency loss. While the study establishes the fundamental adsorption performance of microwave-synthesized $MnFe_2O_4$-modified kaolinite under controlled laboratory conditions, further evaluation under real wastewater matrices, along with scale-up assessments, is required for practical application.

FUNDING

This research received no specific grant from any funding agency in the public, commercial, or not-for-profit sectors.

CONFLICTS OF INTEREST

The authors declare that there is no conflict of interest.

COPYRIGHT

This article is an open-access article distributed under the terms and conditions of the Creative Commons Attribution (CC BY) license (http://creativecommons.org/licenses/by/4.0/).



REFERENCES

Ata, S., Amin, S., Bibi, I., Mohsin, I. U., Islam, A., Mehmood, A., Irshad, S., Al-Fawzan, F. F., Alissa, S. A. and Iqbal, M., Kinetics of methylene blue dye adsorptive removal using halloysite nanocomposite hydrogels. *Zeitschrift Fur Physikalische Chemie*, *236*(3), 373–385(2022). https://doi.org/10.1515/zpch-2021-3075

Babakr, K. A., Aziz, B. K., Shwan, D. M. S., Qader, I. N. and Kaufhold, S., Methylene blue removal by natural clay adsorbent: equilibrium, kinetic and thermodynamic analyses in batch and fixed-bed systems, *React. Kinet., Mech. and Catal.,* 139(2), 1467-1495(2025). https://doi.org/10.1007/s11144-025-03002-y

Baburao, G., Devi, K. V., Balakrishnan, V., Venkatesa Prabhu, V. P., Hariprabhu, M., Selvaraju, S., Shine, K. and Khaled, J. M., Evaluation of detoxification performance of Pithecellobium dulce seed pod powder upon acid treatment: removal of reactive red 195-A dye and kinetic analysis, *Zeitschrift Fur Physikalische Chemie*, 239(6), 885–910(2025). https://doi.org/10.1515/zpch-2024-0879

Barbosa, L. V., Castro, M. S. D. S., Ciuffi, K. J., Nassar, E. J., Marçal, L., Pereira, L. R., Santos, M. F. C., Ambrõsio, S. R., Gomes, P. S. D. S., Nogueira, F. A. R., Santos, R. A. and de Faria, E. H., Kaolinite-titanium nanocomposite applied to the photodegradation of the genotoxic compound cisplatin and the terephthalic acid hydroxylation reaction, *Colloid. Surf. A: Physicochem. Eng. Aspects*, 676, 132144(2023). https://doi.org/10.1016/j.colsurfa.2023.132144

Biswas, S., Rashid, T. U., Debnath, T., Haque, P. and Rahman, M. M., Application of chitosan-clay biocomposite beads for removal of heavy metal and dye from industrial effluent, *J. Compos. Sci.*, 4(1), 16(2020). https://doi.org/10.3390/jcs4010016

Choudhary, N., Yadav, V. K., Ali, H., Ali, D., Almutairi, B. O., Cavalu, S. and Patel, A., Remediation of Methylene Blue Dye from Wastewater by Using Zinc Oxide Nanoparticles Loaded on Nanoclay, *Water* 15(7), 1427(2023). https://doi.org/10.3390/w15071427

Foroutan, R., Mohammadi, R., Razeghi, J., Ahmadi, M. and Ramavandi, B., Amendment of Sargassum oligocystum bio-char with MnFe2O4 and lanthanum MOF obtained from PET waste for fluoride removal: A comparative study, *Environ. Res.*, 251, 118641(2024). https://doi.org/10.1016/j.envres.2024.118641

Grine, O., Andrejkovičová, S., Lazaar, K., Pullar, R. C., Elfil, H., Rocha, F. and Hajjaji, W., Cationic Dye Treatment Using Local Tunisian Iron Tailings for Synthetic and Textile Wastewater, *Chem. Africa*, 8(8), 3595–3611(2025). https://doi.org/10.1007/s42250-025-01354-5

Harinivalli, S., Aparna, S., Anjana, A. S. K., Arockiaveronikka, K., Raja, N., Arthanareeswaran, G. and Mangalaraja, R. V., Hybrid Adsorption–Nanofiltration Using Modified PEI-Based Mixed Matrix Membranes for Efficient Dye Rejection from Wastewater, *Water, Air, Soil Pollut.*, 236(13), 858(2025). https://doi.org/10.1007/s11270-025-08495-w

Hosseini-Bandegharaei, A., Asghari, A., Elahimehr, Z., Nemati, F. and Rajabi, M., Chitosan-derived magnetic nitrogen/selenium-doped porous carbon: A sustainable and high-performance adsorbent for removal of organic pollutants from water and wastewater, *Environ. Technol. Innov.*, 40, 10456(2025). https://doi.org/10.1016/j.eti.2025.104526

Jebanisha, B. and Devi, V. N. M., Biomass-derived activated carbon supported ZnO nanocomposite synthesized via Averrhoa carambola leaf extract for the adsorption of methylene blue dye from aqueous solution, *Sustain. Chem. One World*, 8, 100117(2025). https://doi.org/10.1016/j.scowo.2025.100117

Jiang, J., Deng, S., Kuang, W., Wang, L., Chen, D., Ma, Y. and Yang, W., Highly carboxylate functionalized halloysite nanotube as an efficient and recyclable adsorbent for methylene blue, *Appl. Clay Sci.*, 250, 107292 (2024). https://doi.org/10.1016/j.clay.2024.107292

Karuppaiyan, J., Jeyalakshmi, R., Kiruthika, S., Wadaan, M. A., Farooq, M. F. and Kim, W., A study on the role of surface functional groups of metakaolin in the removal of methylene blue: Characterization, kinetics, modeling and RSM optimization, *Environ. Res.*, 226, 115604(2023). https://doi.org/10.1016/j.envres.2023.115604

Liu, X., Chen, Y., Deng, Z. and Yang, Y., High-performance nanofiltration membrane for dyes removal: Blending Fe3O4-HNTs nanocomposites into poly (vinylidene fluoride) matrix, *J. Dispers. Sci. Technol.*, 42(1), 93–102(2020). https://doi.org/10.1080/01932691.2019.1662308

Loukili, H., Mabrouki, J., Anouzla, A., Kouzi, Y., Alami Younssi, S., Digua, K. and Abrouki, Y., Pre-treated moroccan natural clays: Application to the wastewater treatment of textile industry, *Desalin. Water Treat.*, 240, 124–136(2021). https://doi.org/10.5004/dwt.2021.27644

Milojević-Rakić, M., Gavrilov, N., Janošević Ležaić, A., Uskoković-Marković, S., Nedić Vasiljević, B. and Bajuk-Bogdanović, D., Complementary: Green catalysis over red soil for pollutant removal, *Appl. Clay Sci.*, 262, 107601(2024). https://doi.org/10.1016/j.clay.2024.107601

Mohammad, H. N., Sheshmani, S. and Shahvelayati, A. S., Manganese ferrite-graphite oxide-chitosan nanocomposite for efficient dye removal from aqueous and textile wastewater under UV and sunlight irradiation, *Sci. Rep.*, 15(1), 866(2025). https://doi.org/10.1038/s41598-024-84569-9

Mussttaf, D. J., Abdul-Hamead, A. A. and Othman, F. M., Green synthesis and characterization of CuO, Fe_2O_3 and CuO/Fe_2O_3 compounds investigation, *Res. Eng.*, 22, 102282(2024). https://doi.org/10.1016/j.rineng.2024.102282

Rao, D. P., Devi, V. D., Selvaraju, S., Prabhu, V. P., Kandavalli, S. R., Chitra, M. S., Sivasamy, N. and Pradeep, P., Adsorptive removal of cadmium from electroplating wastewater using hybrid composite of thiol-grafted seed gum of Tamarindus indica and Teff hay biocarbon, *Zeitschrift Fur Physikalische Chemie*, 239(5), 633–654(2025). https://doi.org/10.1515/zpch-2024-0715

Rawat, S. and Ahammed, M. M., Clay-moringa seedcake composite for removal of cationic and anionic dyes, *Chemos.*, 350, 141083(2024). https://doi.org/10.1016/j.chemosphere.2023.141083

Saad, H. E. and Mahmoud, A., Coumarin-modified cellulose as an efficient adsorbent for cationic dye removal from aqueous environments: synthesis, characterization, and adsorption performance, *Sci. Rep.*, 15(1), 32511(2025). https://doi.org/10.1038/s41598-025-17789-2

Sandollah, N. A. S. M., Izaddin, S. M. G. S. A. I., Wan, I. W. N. and Rusmin, R., Adsorption-desorption profile of methylene blue dye on raw and acid activated kaolinite, *Indones. J. Chem.*, 20(4), 755–765(2020). https://doi.org/10.22146/ijc.43552

Sharma, S., Devi, A. and Bhattacharyya, K. G., Photocatalytic Degradation of Methylene Blue in Aqueous Solution with Silver-Kaolinite-Titania Nanocomposite under Visible Light Irradiation, *J. Nanostruct.*, 12(2), 426–445(2022). https://doi.org/10.22052/JNS.2022.02.018

Sharmiladevi, S., Ramesh, N., Prabhu, S. P. and Mayakannan, S., Microwave-assisted functionalized biosorbent preparation using seed gum of Tamarindus indica: characterization and evaluation of Cr (VI) removal potency from tannery effluents, *Biomass Convers. Biorefine.*, 14(12), 13533–13545(2024). https://doi.org/10.1007/s13399-024-05667-2

Shikuku, V. O. and Mishra, T., Adsorption isotherm modeling for methylene blue removal onto magnetic kaolinite clay: a comparison of two-parameter isotherms, *Appl. Water Sci.*, 11(6), 103(2021). https://doi.org/10.1007/s13201-021-01440-2

Subhi, A. M., Al-Najar, J. A. and Noori, W. A. -H. Adsorption of dyes using natural minerals: A review, *Global Nest J.*, 24(3), 451–464(2022). https://doi.org/10.30955/gnj.004325

Suliman, Z. A., Mecha, A. C. and Mwasiagi, J. I., Effect of TiO_2/Fe_2O_3 nanopowder synthesis method on visible light photocatalytic degradation of reactive blue dye, *Heliyon*, 10(8), 29648(2024). https://doi.org/10.1016/j.heliyon.2024.e29648

Turkes, E. and Açıkel, Y., Synthesis and characterization of magnetic halloysite–chitosan nanocomposites: use in the removal of methylene blue in wastewaters, *Int. J. Environ. Sci. Technol.*, 17(3), 1281–1294(2020). https://doi.org/10.1007/s13762-019-02550-w

Yadav, J., Chahal, S., Kashyap, V., Saxena, K. and Kumar, C., Textile Wastewater Treatment for Basic Fuchsin Dye Removal using Highly Efficient Nano Earthenware Clay in Fixed-Bed Reactors, *Water, Air, Soil Pollut.*, 236(8), 512(2025). https://doi.org/10.1007/s11270-025-08155-z